PERGAMON

International Journal of Heat and Mass Transfer 41 (1998) 2929–2945

International Journal of HEAT and MASS TRANSFER

Deposition of tin droplets on a steel plate: simulations and experiments

M. Pasandideh-Fard, R. Bhola, S. Chandra,* J. Mostaghimi

Department of Mechanical and Industrial Engineering, University of Toronto, Toronto, Ontario, M5S 3G8, Canada

Received 22 May 1997; in final form 16 December 1997

Abstract

Impact and solidification of tin droplets on a flat stainless steel plate was studied using both experiments and numerical simulation. In the experiments, tin droplets (2.1 mm diameter) were formed and dropped onto a stainless steel surface whose temperature was varied from 25 to 240 C. Impact of droplets was photographed, and evolution of droplet spread diameter and liquid–solid contact angle measured from photographs. Substrate temperature variation under an impinging droplet was measured. A complete numerical solution of the Navier–Stokes and energy equations, based on a modified SOLA-VOF method, was used to model droplet deformation and solidification and heat transfer in the substrate. Measured values of liquid–solid contact angle were used as a boundary condition for the numerical model. The heat transfer coefficient at the droplet–substrate interface was estimated by matching numerical predictions of the variation of substrate temperature with measurements. Comparison of computer generated images of impacting droplets with photographs showed that the numerical model correctly modelled droplet shape during impact as it simultaneously deformed and solidified. A simple analytical model was developed to predict the maximum spread diameter of a droplet freezing during impact.

Nomenclature

C specific heat
d_s diameter of solid layer
D splat diameter, measured at the splat–substrate interface
D_0 diameter of spherical droplet
D_{max} final splat diameter
F volume of fluid fraction
g acceleration due to gravity
h enthalpy
h_c heat transfer coefficient at droplet/substrate interface
H_f latent heat of fusion
k thermal conductivity
KE_1 initial kinetic energy
q heat flux
s thickness of solid layer
s^* dimensionless thickness of solid layer ($=s/D_0$)
SE_1 droplet surface energy before impact
SE_2 droplet surface energy after impact
t time
t^* dimensionless time ($=V_0 t/D_0$)
t_c time for droplet to reach its maximum spread diameter
T_m droplet melting temperature
T_w substrate temperature
$T_{w,i}$ initial substrate temperature
$\mathbf{V}$ velocity
$\mathbf{V}_0$ droplet impact velocity
W work done in deforming droplet.

Greek symbols

α thermal diffusivity
β $=k/C$
γ surface tension
ΔKE kinetic energy loss due to solidification
θ liquid–solid contact angle
θ_a advancing contact angle
Θ liquid volume fraction
μ viscosity
ν kinematic viscosity

* Corresponding author.

0017-9310/98 $19.00
PII: S0017-9310(98)00023-4

ξ spread factor ($=D/D_0$)
ξ_{max} maximum spread factor
ρ density
Φ source term in energy equation ($= -H_f k_l/C_l$).

Subscripts
l liquid
s solid
w substrate.

Dimensionless numbers
Bi Biot number ($=h_c D_0/k_l$)
Pe Peclet number ($=V_0 D_0/\alpha_l$)
Pr Prandtl number ($=\nu_l/\alpha_l$)
Re Reynolds number ($=V_0 D_0/\nu_l$)
Ste Stefan number ($=C_l(T_m - T_{w,i})/H_f$)
We Weber number ($=\rho_l V_0^2 D_0/\gamma$)

1. Introduction

Thermal spray coating—in which molten droplets of the coating material are propelled at high velocity onto the substrate—is a well established manufacturing process [1]. More recently, new fabrication methods have been developed that use precisely controlled deposition of droplets to produce complex, three-dimensional objects, employing a computer to manipulate the substrate and spray nozzles [2–6]. Such techniques, known variously as 'spray forming' [2, 3], 'microfabrication' [4], 'freeform fabrication' [5], or 'microcasting' [6] offer improved metallurgical performance and reduced manufacturing costs. Property improvements result from rapid solidification of droplets as they impact [7], which gives very fine microstructure and reduced segregation of alloy components. Freeform fabrication also allows production of near net-shaped components, making it materials and energy efficient, enhancing manufacturing flexibility and reducing costs. These technologies, though promising, are still in their infancy. Physical properties such as porosity, microstructure, surface roughness and adhesion strength of coatings or artifacts produced by droplet deposition have been found to be sensitive to a large number of process parameters (e.g., droplet size distribution, velocity, temperature and degree of solidification; substrate material and temperature) which must be optimized by trial and error [1]. Better control of the process requires a fundamental understanding of the fluid flow and heat transfer that occurs during the impact, spreading, and solidification of molten droplets.

Several numerical models have been developed to simulate impact and solidification of molten droplets on a cold surface. Bennett and Poulikakos [8] and Kang et al. [9] studied droplet deposition assuming that solidification starts only after droplet spreading is complete, when the splat is in the form of a disc. The validity of such an assumption depends on the rate of solidification following droplet impact. Zhao et al. [10, 11] studied, using both numerical models and experiments, heat transfer and fluid dynamics during collision of a liquid droplet on a substrate in the case that there is no solidification. Liu et al. [12], Trapaga et al. [13], and Bertagnolli et al. [14] used finite difference models to study the simultaneous spreading and solidification of impacting droplets. They assumed that the substrate was isothermal, and neglected any thermal contact resistance at the liquid–solid interface. The liquid–solid contact angle was assumed to be constant in these studies, with an arbitrarily assigned value. Pasandideh-Fard et al. [15] have shown, however, that the value of the contact angle can significantly influence model predictions. Pasandideh-Fard and Mostaghimi [16] modelled droplet impact assuming heat transfer in both the droplet and substrate to be by one-dimensional heat conduction. They studied the effect of varying thermal contact resistance between the droplet and substrate, and showed that its magnitude can significantly influence droplet spreading. Waldvogel and Poulikakos [17] used a finite element model to simulate spreading and solification during droplet impact. They neglected capillary forces at the liquid–solid contact line and assumed a value of the thermal contact resistance.

Only a few experimental studies have investigated impact of molten droplets. Madejski [18, 19] developed a simple model to predict the maximum splat diameter of a droplet after impact, and compared his predictions with the size of alumina droplets deposited on a cold surface. Inada [20] measured the temperature variation of a plate on which a molten lead droplet was dropped, and noted that the droplet cooling rate was a function of impact velocity. Watanabe et al. [21] photographed impact of *n*-cetane and *n*-eicosane droplets on a cold surface and concluded that in their tests droplets spread completely before solidifying. Fukanuma and Ohmori [22] photographed the impact of tin and zinc droplets and also found that freezing had no influence on droplet spread. Inada and Yang [23] used holographic interferometry to observe droplet–substrate contact during impact of lead droplets on a quartz plate. Liu et al. [24] measured the temperature variation on the upper surface of an impacting metal droplet using a pyrometer, and used these results to estimate the thermal resistance under the drop. However, the response time of their pyrometer (25 m s) was longer than the time taken by the droplet to spread, so that their results are applicable to the period after the droplet had come to rest rather than the duration of impact itself.

None of the models of droplet impact and solidification have been validated rigorously by comparison with experimental results. In part this reflects the scarcity of experimental data. However, such a comparison will likely reveal limitations in the ability of these models to realistically simulate droplet impact dynamics. The

principal difficulty lies in characterizing the surface on which the droplet lands: we have to describe how droplets wet the surface, and accurately estimate the rate of heat transfer from impinging droplet to the surface. These are typically specified in numerical models by two input parameters: the liquid–solid contact angle, and the thermal contact resistance between the substrate and impacting droplets. Lacking information on how to estimate these parameters, modellers have either arbitrarily postulated their value or entirely neglected them, even though it is known that in general such assumptions may significantly influence simulation results [15, 16]. Obtaining such data in practical applications will always be a challenge. It should be noted, though, that in certain circumstances (depending on droplet size, temperature, velocity, material, etc.) it may be valid to disregard the effect of droplet solidification or surface wetting during impact. Pasandideh-Fard et al. [15] showed, using a simple model of droplet spread without solidification, that capillary effects can be neglected during droplet spread if $We \gg \sqrt{Re}$. It would be useful to have a similar criteria to determine when the effect of droplet solidification on impact dynamics is negligible.

This study was undertaken to investigate the capabilities and limitations of numerical models in simulating droplet impact and solidification. Our objectives were to demonstrate that numerical models can realistically simulate droplet impact, provided reasonable estimates of thermal contact resistance and liquid–solid contact angle are available, and to develop guidelines, based on a simple analytical model of droplet impact, for when we can neglect the effect of solidification on droplet spread. We photographed the impact of molten tin droplets on a stainless steel surface and compared the images with droplet shapes predicted by a numerical model. The substrate temperature variation during impact was recorded, and the thermal contact resistance estimated from these results. We also measured the liquid–solid contact angle from photographs and used these measured values as a boundary condition in our model. Substrate temperature was varied in our experiments from 25–240°C. Droplet diameter (2.1 mm), temperature (~240°C), and impact velocity (1.6 m s^{-1}) were held constant.

2. Numerical method

2.1. Fluid flow

Fluid flow in an impacting drop was modelled using a finite difference solution of the Navier–Stokes equations in an axisymmetric system of coordinates, assuming laminar, incompressible flow. The flow Reynolds number (assuming radial flow over a flat plate in the droplet after impact) was estimated to be at most 10^4, too small to induce turbulence. Details of the fluid flow model have been given earlier [15]. The surface profile of the deforming droplet was defined using the 'fractional volume of fluid' scheme [25]. In this method a scalar function, F, is defined whose value is equal to the fractional volume of the cell occupied by the fluid. F is assumed to be unity when a cell is fully occupied by the fluid and zero for an empty cell. Cells with values of $0 < F < 1$ contain a free surface. Normal stresses at a free surface were replaced by an equivalent surface pressure, calculated from the Laplace equation; tangential stresses were neglected. Experimentally measured values of the dynamic liquid–solid contact angle, θ, were prescribed as a boundary condition. Liquid density, viscosity, and surface tension were assumed constant, with values taken from the Metals Handbook [26].

2.2. Heat transfer

Heat transfer in the droplet was modelled by solving the energy equation, neglecting viscous dissipation; densities of liquid and solid tin were assumed constant and equal to each other (the values differ by less than 4%, which would have little influence on droplet flow):

$$\frac{\partial h}{\partial t} + (\mathbf{V}\cdot\nabla)h = \frac{1}{\rho}\nabla\cdot(k\nabla T). \tag{1}$$

Since the energy equation has two dependent variables—temperature T and enthalpy h—we used the enthalpy transforming model [27] to convert the energy equation to one with only one dependent variable: the enthalpy. The final form is [28]

$$\frac{\partial h}{\partial t} + (\mathbf{V}\cdot\nabla)h = \frac{1}{\rho}\nabla\cdot(\beta\nabla h) + \frac{1}{\rho}\nabla^2\Phi \tag{2}$$

where in the solid phase:

$$h \leqslant 0; \quad \beta = \frac{k_s}{C_s}, \quad \Phi = 0 \tag{3a}$$

at the liquid–solid interface:

$$0 < h < H_f; \quad \beta = 0; \quad \Phi = 0 \tag{3b}$$

and in the liquid phase:

$$h \geqslant H_f; \quad \beta = \frac{k_l}{C_l}; \quad \Phi = -\frac{H_f k_l}{C_l} \tag{3c}$$

where we have introduced a new source term Φ. The energy equation now has only one dependent variable, the enthalpy h. The relationship between temperature and enthalpy is given by

$$T = T_m + \frac{1}{k}(h\beta + \Phi) \tag{4}$$

where T_m is the melting point of the droplet. Heat transfer within the substrate is by conduction only. The governing equation is:

$$\rho_w C_w \frac{\partial T_w}{\partial t} = \nabla\cdot(k_w \nabla T_w). \tag{5}$$

The free surface of the droplet was assumed to be adiabatic: estimates of heat loss by natural convection from the droplet surface to the ambient air showed them to be three orders of magnitude lower than that to the substrate. Thermal contact resistance between the droplet and substrate was quantified using a heat transfer coefficient (h_c) defined by:

$$h_c = \frac{q}{(T - T_w)_{z=0}} \tag{6}$$

where q is the heat flux between the droplet and substrate. Values of h_c were provided as an input to the model. Though in principle h_c could vary with time and/or position on the interface, we used, for reasons discussed below, a single constant value of $h_c = 2 \times 10^5$ W m^{-2} K^{-1} in all our simulations.

2.3. Solidification

In the presence of a solid phase, computations of the velocity field have to account for the presence of a moving, irregularly shaped solidification front on which the relevant boundary conditions have to be applied. We treat the solidified regions of the domain using a modified version of the fixed velocity method [29]. In this approach, a liquid volume fraction Θ is defined such that $\Theta = 1$ for a cell containing only liquid, $\Theta = 0$ for a cell containing only solid, and $0 < \Theta < 1$ for a cell containing a portion of the solidification front. Normal and tangential velocities on the faces of cells containing only solidified material are set to zero. The solidification front was represented using a two phase continuum model to modify the continuity and momentum equations. The final modified equations are [30]:

$$\nabla \cdot (\Theta \mathbf{V}) = 0 \tag{7}$$

$$\frac{\partial(\Theta \mathbf{V})}{\partial t} + (\Theta \mathbf{V} \cdot \nabla) = \frac{-\Theta}{\rho} \nabla P + \Theta \nu \nabla^2 \mathbf{V} + \Theta \mathbf{g} \tag{8}$$

$$\frac{\partial F}{\partial t} + (\Theta \mathbf{V} \cdot \nabla) F = 0. \tag{9}$$

The solidification front is treated as a no-slip wall on which the zero velocities are applied. When the free surface of the droplet intersects with the solidification front, the contact angle is prescribed along the contact line, as described before.

2.4. Numerical procedure

The modified Navier–Stokes equations were solved on an Eulerian rectangular, staggered mesh in an axisymmetric coordinate system using the modified SOLA-VOF method. The finite difference expressions for equations (7) and (8) were derived by differencing these equations in a manner similar to that used in one-phase flow formulations. The finite difference expressions for the one-phase flow equations are a special case of the two-phase flow equations when $\Theta = 1$. The computational procedure for advancing the solution through one time step is as follows:

(1) From time level n values, the velocity and pressure fields as well as F are calculated at time level $n+1$ in accordance with the modified SOLA-VOF algorithm.
(2) Given the droplet enthalpy and substrate temperature fields at time level n, equations (2) and (5) are solved to obtain the new enthalpy field in the droplet and the new temperature field in the substrate. Temperatures in the droplet can then be calculated from equation (4).
(3) New values of the liquid volume fraction Θ are calculated from the enthalpy field in the droplet by using equation (3a–c) in conjunction with an algorithm described by Voller and Cross [31]. In this algorithm, while a change of phase is occurring in the sub-region of a computational cell, the rate of change in the cell enthalpy equals the velocity of the phase change front across the subregion multiplied by the latent heat of fusion.
(4) Flow and thermal boundary conditions are imposed on the free surface, at the solidification front, and the boundaries of the computational domain. In particular, the heat transfer coefficient at the droplet–substrate interface is applied by using equation (6) to calculate the heat flux from the droplet. This value of q is then used to update temperature boundary conditions along the bottom surface of the droplet and the upper plane of the substrate.

Repetition of these steps allowed advancing the solution through an arbitrary time interval. The droplet was discretized using a uniform computational mesh, with a grid spacing equal to 1/30 of the droplet radius. The substrate mesh had the same resolution, and was extended far enough that its boundaries could be assumed to be at constant temperature. Numerical computations were performed on a Sun (SPARC 10) workstation. Typical CPU times ranged from 2 to 5 h.

3. Experimental method

Figure 1 is a schematic diagram of the apparatus used for creating in droplets and photographing their impact on the test surface. The droplet generator consisted of a 76.2 mm diameter, 76.2 mm long stainless steel cylinder, in which was machined a 38.1 mm diameter, 60.3 mm deep cavity. The cylinder was heated by four 100 W cartridge heaters inserted in it, which were regulated by a temperature controller. A 1 mm outer diameter stainless steel needle was fitted through a hole in the bottom of the cavity. A pointed stainless steel rod attached to a

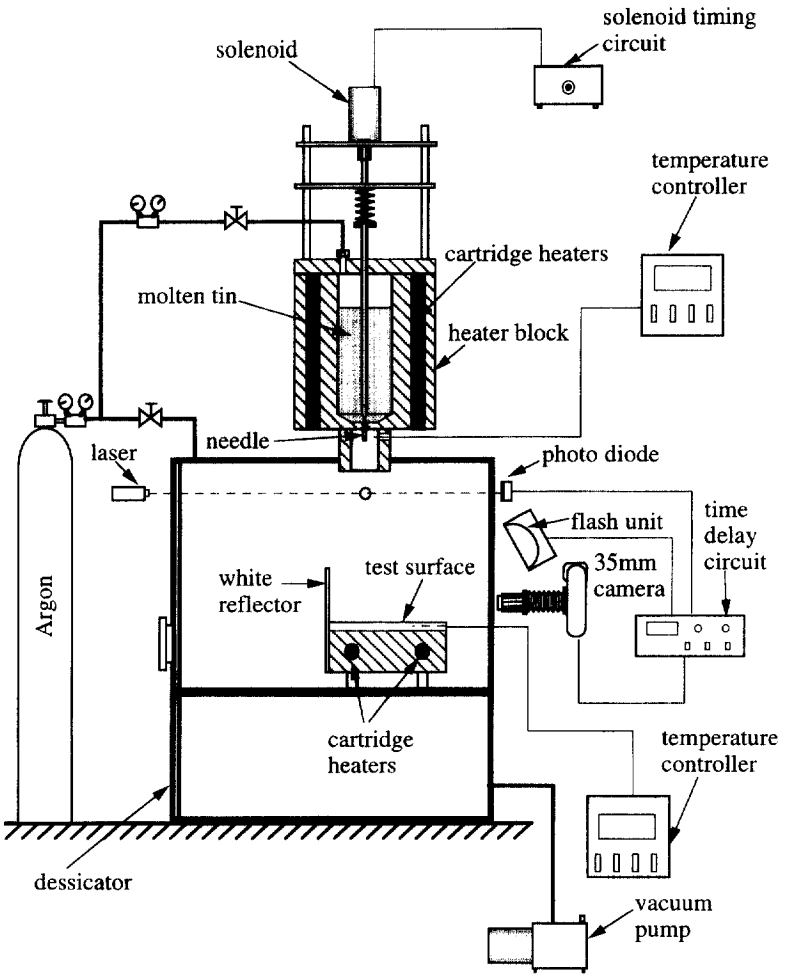

Fig. 1. Schematic diagram of the experimental apparatus.

solenoid plugged the entrance to the needle. Activating the solenoid lifted the rod, uncovering the opening to the needle and allowing molten tin to flow through. The solenoid lift duration could be varied from 0.1–1 s by an electronic timing circuit.

The cavity in the droplet generator was filled with tin pellets (purchased from Aldrich Chemical Co., 99.8% purity). The temperature of the droplet generator was fixed at 240°C; the melting point of tin (T_m) is 232°C. Calculations of heat loss from the droplet during its fall showed that it would cool by approximately 6°C, so that it remained entirely liquid at the moment of impact. The surface tension of tin is too high for it to flow through the needle under its own weight. The cavity was therefore pressurized to about 10 kPa above atmospheric pressure with argon gas from a cylinder, which was sufficient to force molten tin through the needle. A single droplet, 2.1 ± 0.04 mm in diameter, formed and detached from the needle tip when the solenoid was activated. The test surface was a 50.8 mm square by 6.35 mm thick stainless steel plate polished with 600 grit energy cloth and metal polish. This surface was mounted onto a copper block heated by two cartridge heaters, whose temperature was controlled by a second temperature controller. The test surface was placed 135 mm below the needle tip. The velocity of droplets impacting on the surface, measured from photographs of droplets taken prior to impact, was 1.60 ± 0.002 m s^{-1}.

Tin oxidizes readily in air when heated. The presence of an oxide layer on the surface of droplets formed in air was found to severely distort their shape, so that they were not spherical after detaching from the needle tip. To avoid contaminating the tin, the test surface on which droplets landed was contained in an inert argon atmosphere. The droplet generator was mounted on top of an acrylic dessicator ($0.3 \times 0.3 \times 0.3$ m in size), which was first evacuated with a vacuum pump and then filled with argon gas from a cylinder. A small flow of argon was

maintained during the experiment to prevent air leaking into the chamber.

A single-shot flash-photographic technique was used to capture droplet impact. An electronic flash unit was used to take a single 35 mm photograph of a droplet at one instant after impact. The method has been described in detail by Chandra and Avedisian [32]. As a droplet fell towards the surface it interrupted the beam of a 0.5 mW He–He laser. A photo diode detected this interruption and signalled the time delay circuit, which first opened the shutter of a 35 mm camera and then after a preset delay triggered the flash unit, producing an 8 μs duration flash. Impacting droplets were photographed at different stages of deformation by varying the time delay before triggering the flash, and the entire impact process pieced together from these photographs.

Measurements of droplet dimensions were made from photographs, using the image of a 3 mm steel ball bearing as a calibration scale. A photographic enlarger was used to project images of droplets on a white surface, from which measurements of droplet diameter were made with a resolution of ± 0.01 mm. Contact angle measurements were made from photographic prints by drawing a line tangential to the liquid–air interface, and measuring the angle between this line and the solid surface. Details of this measurement method have been given by Pasandideh-Fard et al. [15]. Contact angle measurements were repeatable within $\pm 3^\circ$.

We measured surface temperature variation during droplet impact using a commercially available fast-response (10 μs) stainless steel sheathed chromel–alumel thermocouple (E12-3-K, Nanmac Inc., Framingham, MA). The thermocouple sheath was inserted vertically through a hole in the stainless steel substrate, held rigidly in place by a pipe fitting screwed into the heater block, and the exposed thermocouple junction ground flush with the surface. The temperature sensor on the surface was located at the point of droplet impact. When a molten tin droplet landed on the thermocouple its output was amplified, and recorded using a data acquisition system. Temperature measurements were estimated to be accurate within $\pm 1^\circ$C.

4. Results and discussion

Figure 2 shows photographs of the impact of 2.1 mm diameter tin droplets, with an initial temperature of approximately 240°C and velocity of 1.6 m s^{-1}, impacting on a stainless steel surface. Each column of photographs in Fig. 2 shows successive stages of impact on surfaces at temperatures of 25, 150 and 240°C, respectively. The time of each image (t), measured from the instant of first contact with the surface, is shown. The reflection of each drop in the polished stainless steel surface can be seen in the photographs.

Droplets falling on a surface at 25°C spread after impact to their maximum extension at approximately $t = 3.0$ m s (see Fig. 2), after which surface tension forces prevented any further spread. The edges of the drop were drawn back by surface tension for $t > 4.5$ m s, decreasing the splat diameter. The edges of the droplet solidified by $t = 7$ m s, after which the splat diameter did not change. However, the center of the splat was still liquid, and continued to flow until $t = 20$ m s. When the initial surface temperature ($T_{w,i}$) was raised to 150°C, the initial stages of impact appeared qualitatively similar to that with $T_{w,i} = 25^\circ$C (see Fig. 2). However, solidification was slower on the hotter surface, and the droplet remained liquid for a longer period of time, so that the maximum splat diameter was slightly larger. Surface tension forces caused a slight recoil of the drop off the surface ($t = 11$ m s), and also smoothed out the surface. At $T_{w,i} = 240^\circ$C, the surface was at the same temperature as the initial droplet temperature: impact was isothermal and the droplet remained liquid throughout impact. After a droplet spread on the surface to its maximum extent ($t = 3$ ms), surface tension and viscous forces overcame liquid inertia, so that fluid accumulated at the leading edge of the splat and it started pulling back, eventually rising off the surface. It then fell back and reached its equilibrium state, shaped like a truncated sphere, after $t > 500$ m s.

Predictions from the computer model of droplet impact are sensitive to the values of two input parameters: the liquid–solid contact angle (θ), and the heat transfer coefficient (h_c) at the droplet–substrate interface. We estimated both of these from experimental measurements. Figure 3 shows the evolution of contact angle, measured from photographs of impacting droplets. The advancing contact angle, during outward spreading of the droplet ($t < 4$ m s), was approximately constant at $140 \pm 10^\circ$. The receding contact angle, during droplet recoil, was somewhat smaller ($\sim 125^\circ$) on a surface at 240°C (see Fig. 3). The definition of a receding contact angle was rather ambiguous in the case of $T_{w,i} = 25^\circ$C and $T_{w,i} = 150^\circ$C, since the layer in contact with the hot surface solidified shortly after impact and stopped moving (see Fig. 2). However, the liquid above this solidified layer continues to move. We therefore defined a contact angle between a line drawn tangential to the edge of the liquid portion and the plane of the solid substrate: these values are shown in Fig. 3. These measurements, though admittedly not very accurate, do confirm that the contact angle was small ($\sim 10^\circ$) during recoil—as would be expected for a melt wetting its own solid—and relatively constant. In the model we used a constant value of $\theta = 10^\circ$ for $t > 10$ m s.

The heat transfer coefficient (h_c) was estimated by comparing the measured substrate temperature variation during droplet impact with results from the computer model, and adjusting the thermal contact resistance value to obtain the best agreement. The measured evolution of

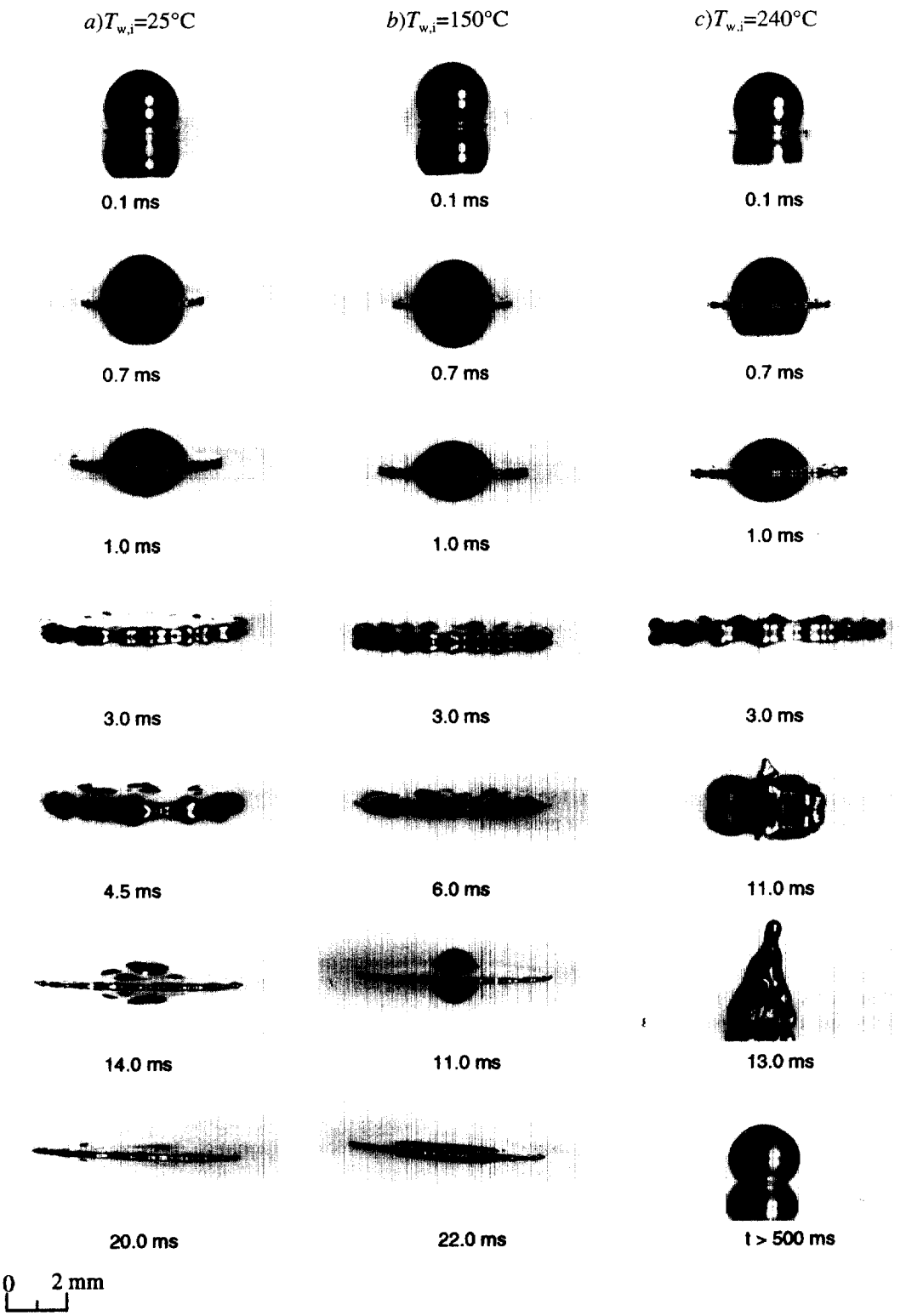

Fig. 2. Impact of molten tin drops on a stainless steel surface at an initial temperature of (a) 25 C, (b) 150 C, (c) 240 C.

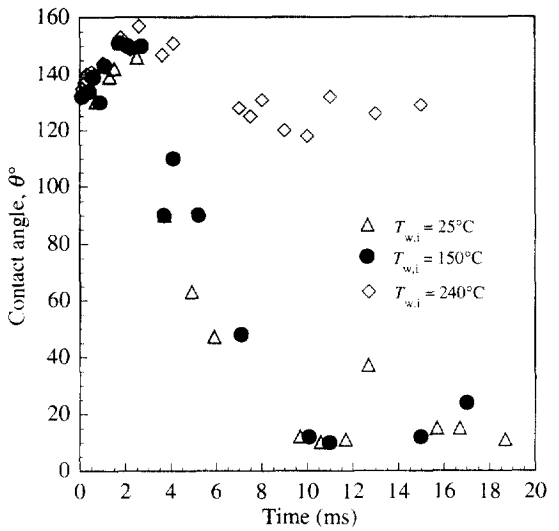

Fig. 3. Liquid–solid contact angle variation during the impact of molten tin drops on a stainless-steel surface at initial temperature $T_{w,i}$.

surface temperature, set prior to droplet deposition at 25 and 150 C, respectively, is shown in Fig. 4(a) and (b). The substrate temperature was measured by a thermocouple placed at the point the drop impacted. A surface initially at 25 C was heated to 160 C in less than 1 m s (Fig. 4(a)); its temperature remained nearly constant for the next few milliseconds, after which it began to cool. When the initial substrate temperature was set at 150°C the peak temperature rose to 225°C (Fig. 4(b)). The predicted temperature variation is shown by solid lines in Fig. 4(a) and (b). At an initial surface temperature of 25 C satisfactory agreement between the measured and predicted values was obtained using a single, constant value of the heat transfer coefficient, $h_c = 10^6$ W m^{-2} K^{-1} for $t < 3$ m s (see Fig. 4(a)). However, at later times ($t > 6$ m s) a lower value of $h_c = 2 \times 10^5$ W m^{-2} K^{-1} gave better predictions of substrate temperature. Liu et al. [24] have shown that the heat transfer coefficient decreases as a droplet solidifies, because of higher resistance to heat transfer at a solid–solid interface than at a solid–liquid interface. It should also be noted that our temperature measurement was done at a single point: it is likely that the local heat transfer coefficient varies with position under the splat. With an initial surface temperature of 150 C the surface temperature variation was best simulated using a high heat transfer coefficient, $h_c = 10^7$ W m^{-2} K^{-1} (see Fig. 4(b)). This result was expected, since droplet solidification would be delayed on the hotter surface, reducing contact resistance.

Comparison of computed droplet shapes during impact with photographs showed that using the range of heat transfer coefficient values obtained from temperature measurements resulted in reasonably good predictions. The rate of droplet spreading was quantified by measuring the splat diameter (D) at successive stages during droplet deformation. Normalizing D by the initial droplet diameter (D_0) yields the so-called 'spread factor', $\xi = D(t)/D_0$. Measured values of ξ during the impact of droplets on surfaces with initial temperatures of 25 and 150 C are shown in Fig. 5(a) and (b), respectively. Using a single value of heat transfer coefficient $h_c = 10^6$ W m^{-2} K^{-1} gave good predictions for ξ for $t < 1$ m s. At that time, however, the simulated droplet solidified completely and did not spread further. Decreasing h_c to 2×10^5 W m^{-2} K^{-1} in the model reduced the droplet solidification rate, and improved agreement between pre-

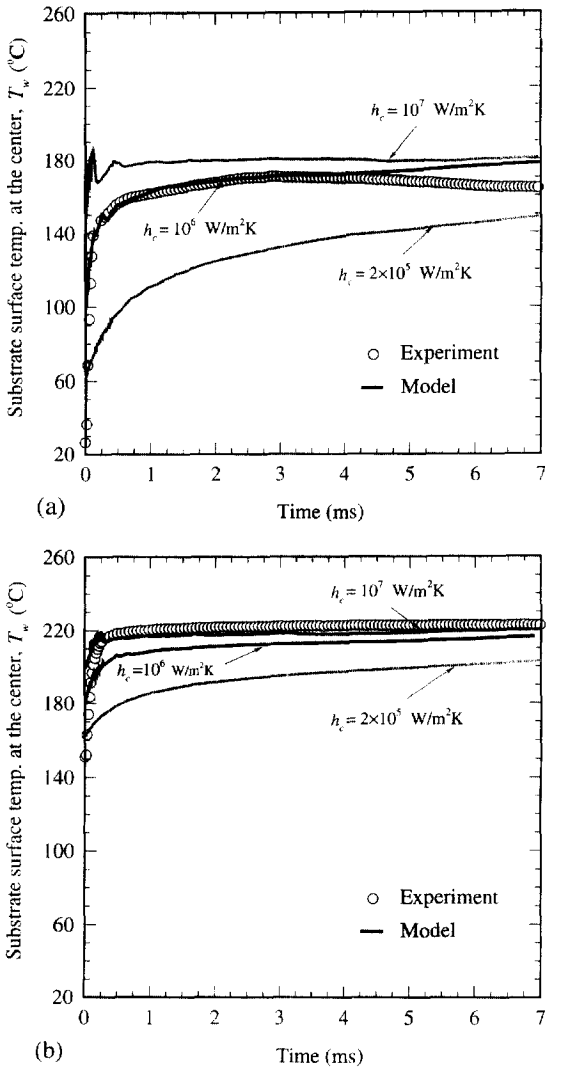

Fig. 4. Substrate surface temperature variation during the impact of a molten tin droplet on a stainless-steel surface initially at (a) 25°C, (b) 150°C.

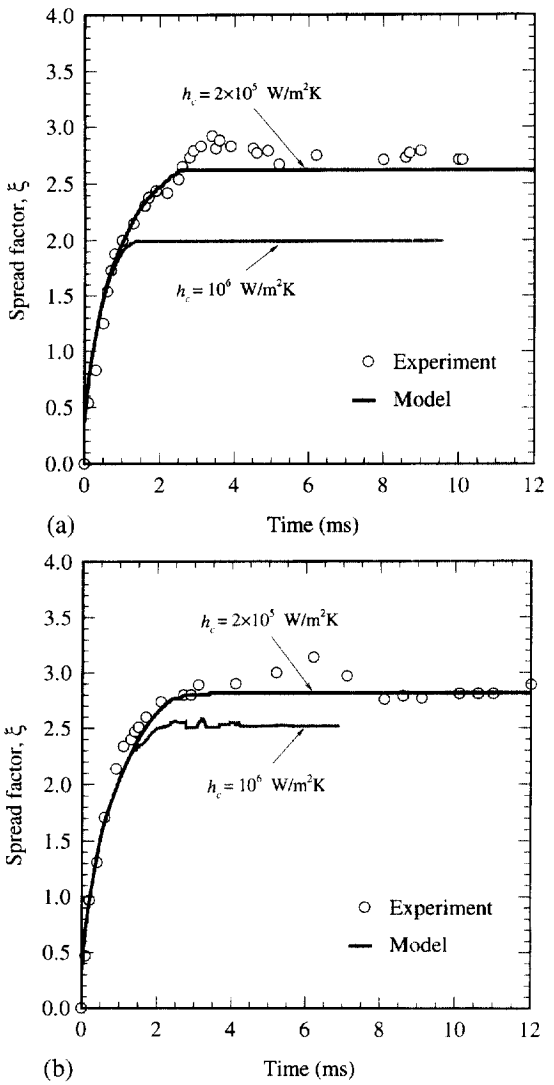

Fig. 5. Evolution of spread factor during impact of tin droplets on a stainless steel surface initially at (a) 25°C, (b) 150°C.

dicted and measured values of ξ. The same heat transfer coefficient also gave good predictions for the spread of a droplet on surface at 150°C (Fig. 5(b)). The range of heat transfer coefficient obtained by these two different methods—matching either the measured surface temperature variation or the droplet spread rate with results from the model—appears to confirm earlier observations [24] that h_c varies during impact. Better agreement between experimental and numerical results could have been obtained by using local heat transfer coefficients that varied with time and position, rather than an average, constant value. However, we did not attempt to do this since we had no independent method of justifying any assumed variation of h_c. All calculations in this paper were performed, therefore, using a constant heat transfer coefficient value of 2×10^5 W m^{-2} K^{-1}.

Computer generated images of impacting droplets are compared with photographs taken at the same time after impact in Figs. 6–10. Droplets were photographed with the camera pointing down at the surface, inclined at an angle of approximately 30° below the horizontal. Impact on a surface with initial temperature $T_{w,i} = 240$°C is shown in Fig. 6. In this case impact was isothermal, and there was no solidification. Agreement between the predicted droplet shapes and photographs was in general good during droplet spreading ($t < 4$ ms). Waves formed around the periphery of the drop (see $t = 9.5$ ms) as a result of the Rayleigh–Taylor instability, which occurs when one fluid is accelerated into another of different density. The model, which was two-dimensional and assumed axisymmetry, was not capable of simulating this instability: a three-dimensional model is necessary to reproduce such a flow. It did, however, accurately predict droplet recoil off the surface ($t = 15$ ms).

Figure 7 shows computer predictions of the shape of droplets impacting on a surface with $T_{w,i} = 25$°C, in which case the extent of solidification during impact was significant. Calculated velocity and temperature distributions inside droplets, at the same times following impact as those in Fig. 7, are displayed in Fig. 8. The solidified layer (seen in yellow in Fig. 8) was thickest at the center of the splat, which first contacted the surface, and along its edge, which was nearest to the surrounding cold plate. Results from the computation showed that the heat flux from the droplet to the substrate increases with radial distance from the center. Solidification along the edge prevented further spread of the drop (see Fig. 8, $t = 4.5$ ms). However, there remained a film of molten tin above the solid layer, which recoiled and flowed back towards the center of the splat. This movement can be seen in the photographs of Fig. 7 (see $t = 7.5$ and 12 ms). By $t = 12$ ms almost all the tin had frozen. Solidification was rapid enough that the splat surface did not have enough time to become even, but had a number of craters left in it.

Similar photographs and computer generated images of a droplet landing on a surface with $T_{w,i} = 150$°C are shown in Figs. 9 and 10. Growth of the frozen layer was much slower in this case, because of the hotter substrate. However, the periphery of the splat solidified by $t = 8.5$ ms. Close inspection of the photographs in Fig. 9 at $t = 8.5$ ms confirms that the splat edges were solid; surface tension would have been evened out the irregularities seen around the fringes if they remained liquid. Most of the droplet remained liquid as late as $t = 15$ ms, leading to a large recoil towards the center. The surface of the splat was smooth in this case, because of the slower solidification (see Fig. 9, $t = 15$ ms).

Droplet solidification may or may not influence its spread, depending on a number of parameters such as

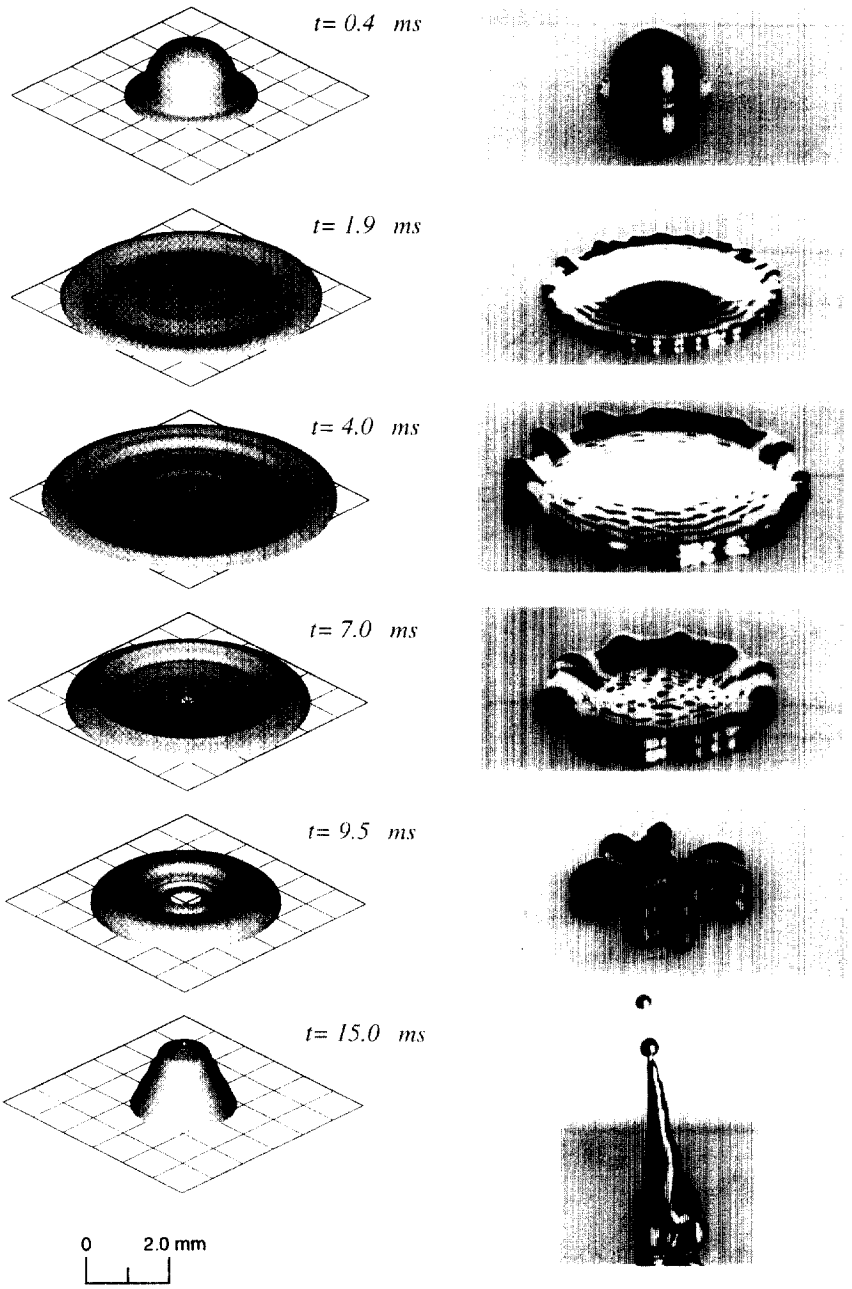

Fig. 6. Computer generated images and photographs of the impact of tin droplets on a surface initially at 240°C.

droplet material, temperature, and velocity, or substrate material and temperature. Droplet impact simulations are greatly simplified if the rate of solidification is insufficient to inhibit droplet spreading, because it is then necessary to solve only the equations of fluid flow, assuming that droplet freezing commences only after it has come to rest [8, 9]. We developed a simple criterion to determine whether droplet effects are negligible by extending the analytical droplet impact model of Pasandideh-Fard et al. [15]. The model predicts that the time taken (t_c) for a liquid droplet to spread to its maximum extent is:

$$t_c = \frac{8D_0}{3\mathbf{V}_0} \tag{10}$$

where $\mathbf{V}_0$ is the impact velocity. Equation (10) predicts

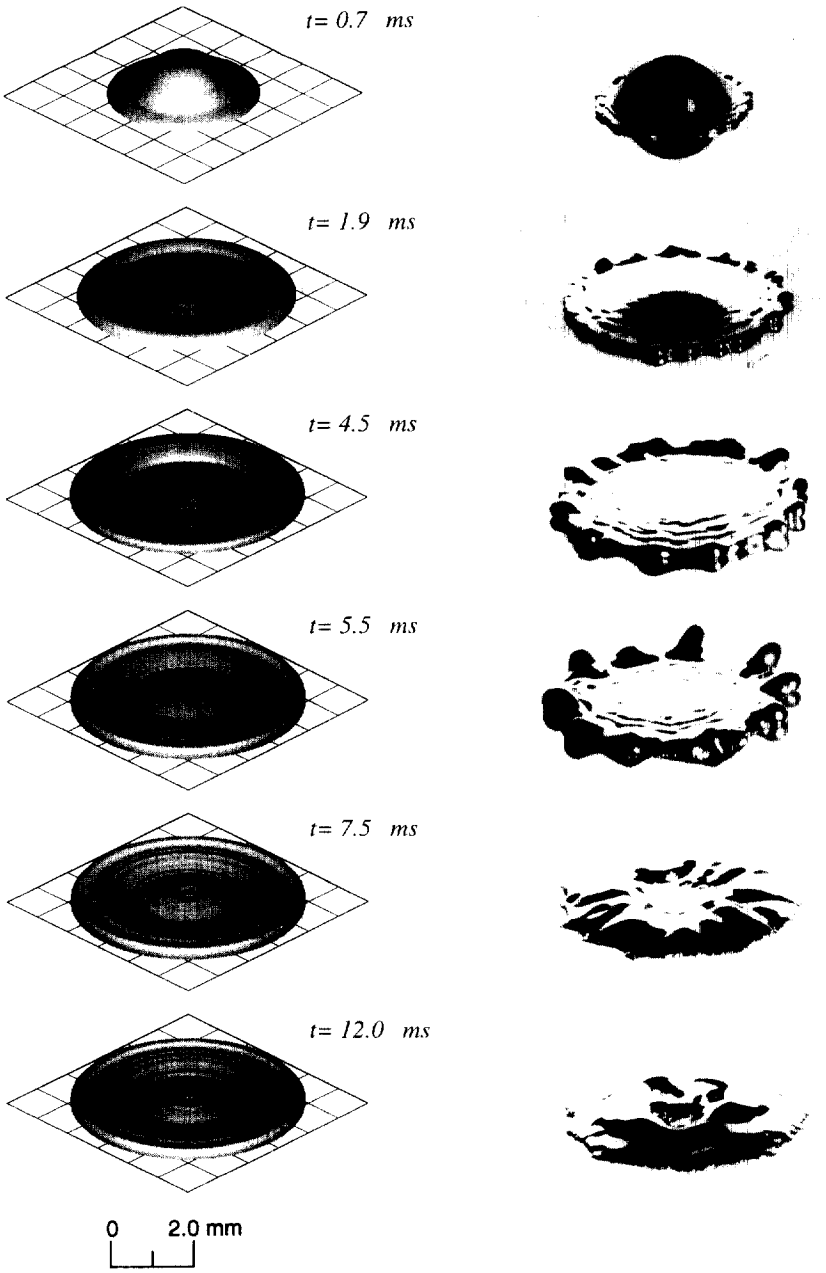

Fig. 7. Computer generated images and photographs of the impact of tin droplets on a surface initially at 25°C.

t_c = 3.5 ms, which is very close to the observed value (see Fig. (5a) and (b)).

The maximum spread diameter of a droplet (D_{max}) can be predicted by equating droplet energy before and after impact, accounting for energy dissipated during impact. The initial kinetic energy (KE_1) and surface energy (SE_1) of a liquid droplet before impact are [15]:

$$KE_1 = \left(\frac{1}{2}\rho \mathbf{V}_0^2\right)\left(\frac{\pi}{6}D_0^3\right) \tag{11}$$

$$SE_1 = \pi D_0^2 \gamma. \tag{12}$$

After impact, when the droplet is at its maximum extension, the kinetic energy is zero and the surface energy (SE_2) is:

$$SE_2 = \frac{\pi}{4} D_{max}^2 \gamma (1 - \cos\theta_a) \tag{13}$$

where θ_a is the advancing liquid–solid contact angle. The work done in deforming the droplet against viscosity (W) is [15]:

$$W = \frac{\pi}{3} \rho V_0^2 D_0 D_{max}^2 \frac{1}{\sqrt{Re}} \tag{14}$$

Re is the Reynolds number ($Re = V_0 D_0/\nu_l$).

The effect of droplet solidification on the maximum spread diameter can be determined by assuming that all the kinetic energy stored in the solidified layer is lost. If the solid layer has average thickness s and diameter d_s when the splat is at its maximum extension, then the loss of kinetic energy (ΔKE) is approximated by:

$$\Delta KE = \left(\frac{\pi}{4} d_s^2 s\right)\left(\frac{1}{2}\rho V_0^2\right) \tag{15}$$

d_s varies from 0 to D_{max}: a reasonable estimate of its average value is $d_s \sim D_{max}/2$. Substituting equations (11)–(15) in the energy balance $KE_1 + SE_1 = SE_2 + W + \Delta KE$ yields:

$$\xi_{max} = \sqrt{\frac{We + 12}{\frac{3}{8} We\, s^* + 3(1 - \cos\theta_a) + 4\frac{We}{\sqrt{Re}}}}. \tag{16}$$

We is the Weber number ($We = \rho_l D_0 V_0^2/\gamma$) and s^* is the dimensionless solid layer thickness ($s^* = s/D_0$). If we make the simplifying assumptions that: heat transfer is by one-dimensional heat conduction; the substrate is isothermal; thermal contact resistance is negligible; and the Stefan number ($Ste = C_l(T_m - T_{w,i})/H_f$) is small; s^* increases with dimensionless time ($t^* = tV_0/D_0$) as [33]:

$$s^* = \sqrt{2t^* \frac{Ste}{Pe}} \tag{17}$$

where Pe is the Peclet number ($Pe = V_0 D_0/\alpha_l$). Combining equations (16) and (17) and setting $t^* = 2.67$ [from equation (10), the time at which a droplet has deformed to its greatest extent] gives an estimate of the maximum spread factor for a droplet that is solidifying during impact:

$$\xi_{max} = \sqrt{\frac{We + 12}{3(1 - \cos\theta) + 4(We/\sqrt{Re}) + We\sqrt{(3Ste)/(4Pe)}}}. \tag{18}$$

The magnitude of the term $We\sqrt{(3Ste)/(4Pe)}$ in equation (18) determines whether solidification influences droplet spread. Comparison with the other two terms in the denominator shows that the kinetic energy loss due to solidification will be too small to affect the extent of droplet deformation if $\sqrt{Ste/Pr} \ll 1$ (where the Prandtl number $Pr = Pe/Re = \nu_l/\alpha_l$). For a tin droplet impacting on a surface at 25°C, $Ste = 0.774$, $Pr = 7.3 \times 10^{-3}$, and $\sqrt{Ste/Pr} = 10.3$: clearly solidification may influence droplet spread. However, substituting our experimental values of $We = 71$, $Re = 1.2 \times 10^4$ and $\theta_a = 140°$ in equation (18) gives $\xi_{max} = 2.5$, much smaller than the measured value of 2.9. The discrepancy arises because the assumptions made in deriving equation (17), that thermal contact resistance at the interface is negligible, and that the substrate is isothermal, are not valid in our experiments. The Biot number ($Bi = h_c D_0/k_l$) is relatively small (approximately 6.8 for $h_c = 2 \times 10^5$ W m^{-2} K^{-1}), showing that the thermal contact resistance is significant. Analysis of splat cooling [34] has shown that the effects of thermal contact resistance are negligible only if $Bi > 30$. Equation (17) therefore only gives an upper bound on the thickness of the solidified layer; the actual magnitude may be significantly lower.

A more realistic value of s^* can be calculated using an analytical model developed by Garcia et al. [35] that predicts the rate of solidification of molten metal in contact with a cold surface. The model assumes: heat transfer in the droplet is by one-dimensional heat conduction; the droplet and substrate are semi-infinite bodies suddenly brought into contact; and thermal contact resistance at the droplet–substrate interface is constant. The calculated variation of s^*, using a constant value of $h_c = 2 \times 10^5$ W m^{-2} K^{-1}, is shown in Fig. 11. The thickness of the solid layer predicted by the numerical model (see Fig. 8), averaged over the splat diameter, is also shown. Results from the analytical model, which now includes the influence of thermal contact resistance and substrate heating, agree well with predictions from the numerical calculation. Values of s^* calculated from equation (17), where these effects are neglected, are seen to be much larger.

We calculated ξ_{max} from equation (16) for droplets impacting on substrates at several different temperatures. Values of s^* for $T_{w,i} = 25$°C were obtained from Fig. 11 at $t^* = 2.67$, which gives an estimate of the thickness of the solid layer formed in the time the droplet takes to reach its maximum spread. Similar computations were done for other substrate temperatures. Predicted values of ξ_{max} agreed closely with those measured. We calculated: $\xi_{max} = 3.24$ (compared to the measured value of $\xi_{max} = 3.3$) for $T_{w,i} = 240$°C (for which there was no solidification and $s^* = 0$); $\xi_{max} = 3.17$ (measured $\xi_{max} = 3.1$) for $T_{w,i} = 150$°C; and $\xi_{max} = 3.02$ (measured $\xi_{max} = 2.9$) for $T_{w,i} = 25$°C.

5. Conclusions

We studied the impact and solidification of tin droplets on a flat stainless steel substrate using both experiments and numerical modeling. Comparison of computer generated images of deforming droplets with photographs showed that the model correctly modelled droplet shape

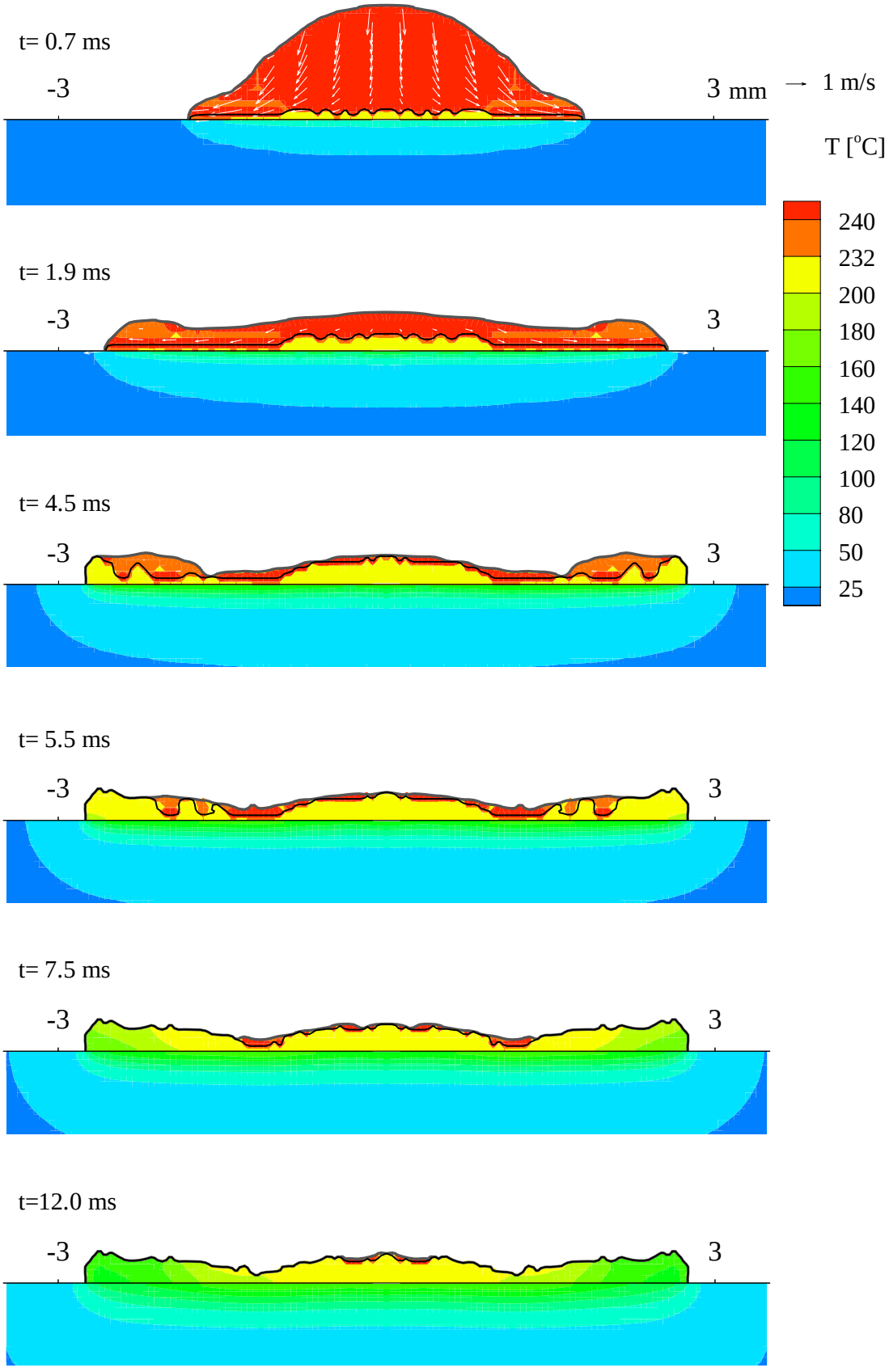

Fig. 8. Calculated velocity and temperature distributions inside a tin droplet impacting a surface initially at 25°C.

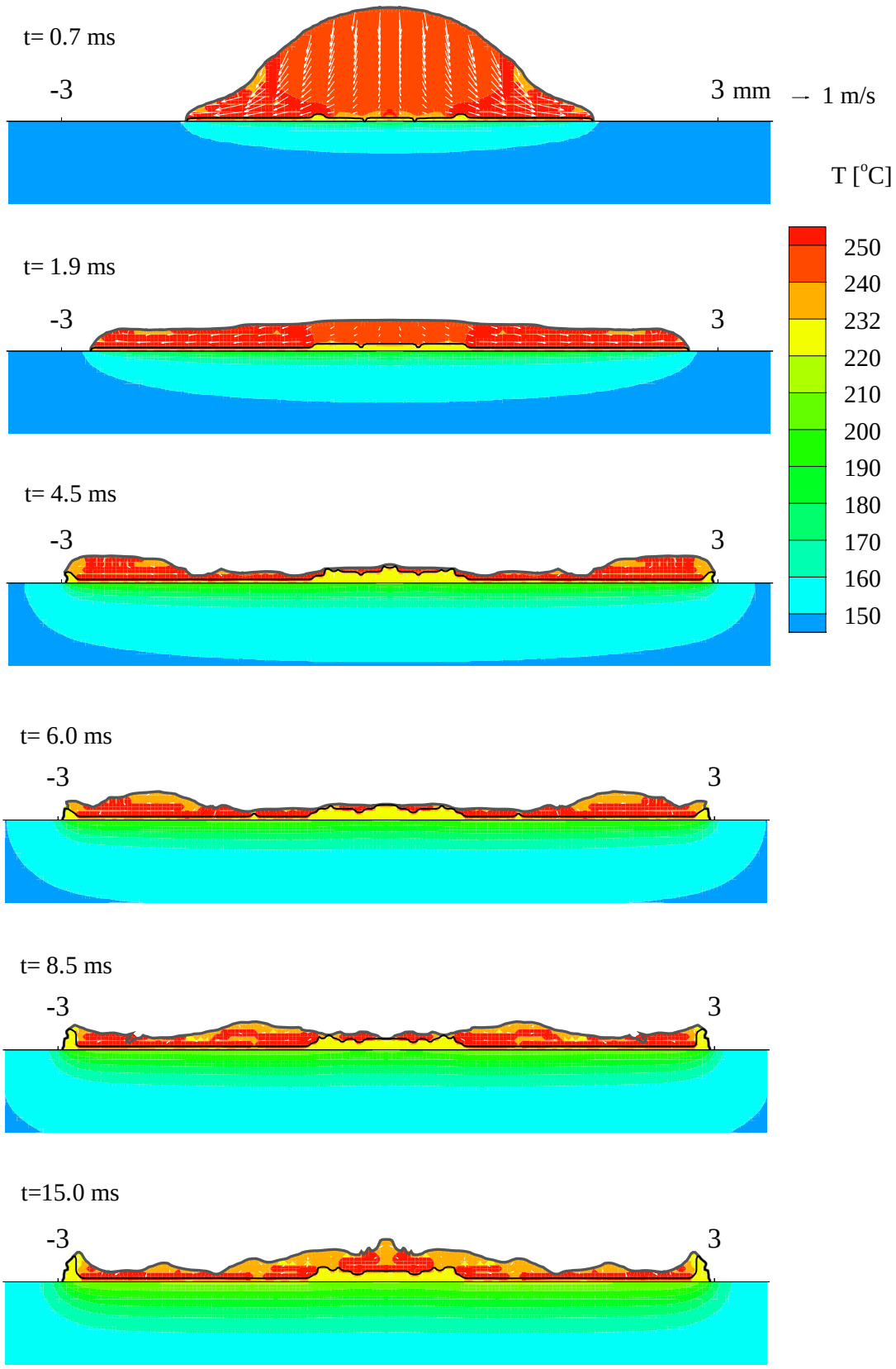

Fig. 10. Calculated velocity and temperature distributions inside a tin droplet impacting a surface initially at 150°C.

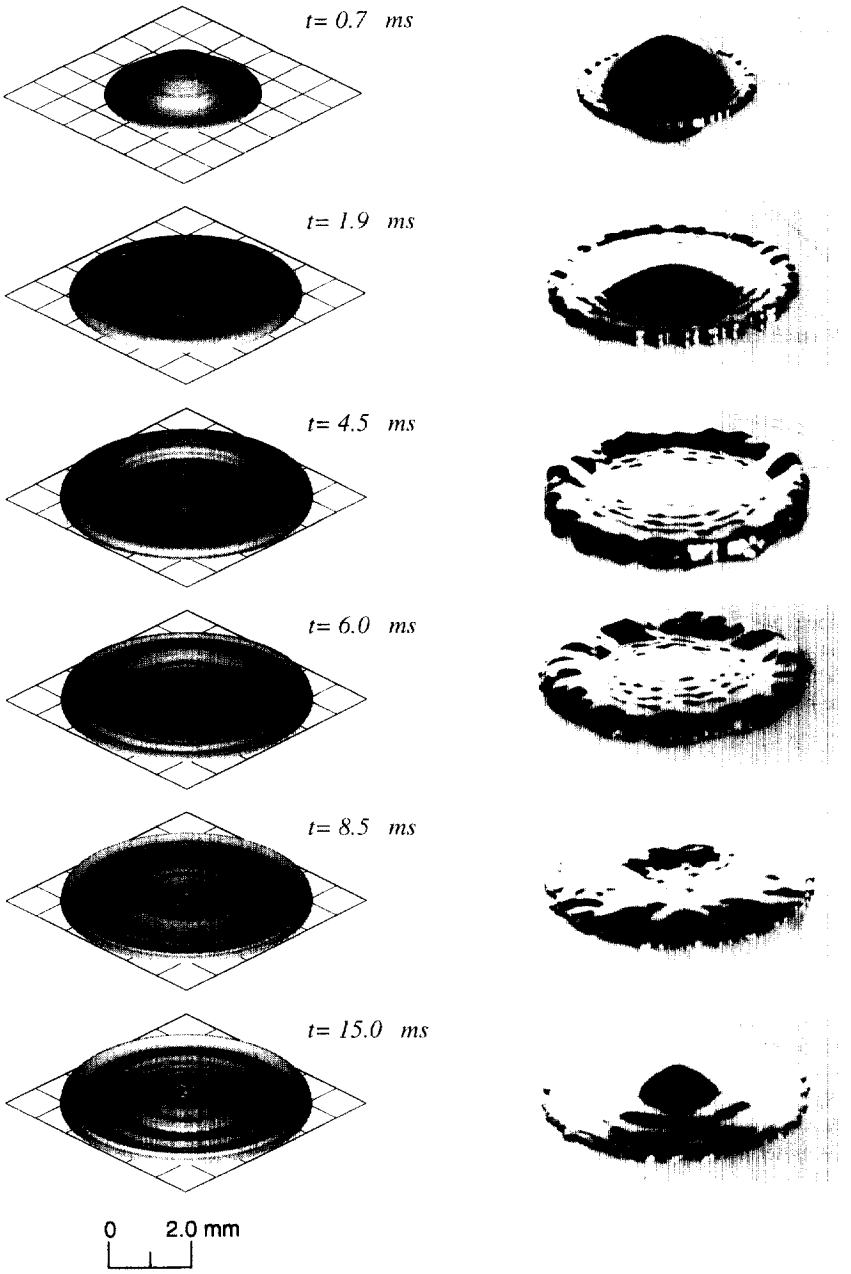

Fig. 9. Computer generated images and photographs of the impact of tin droplets on a surface initially at 150 C.

during impact. The value of contact resistance between the tin droplet and stainless steel substrate was estimated by matching numerical predictions of substrate temperature with experimental measurements. Reasonably accurate simulations of droplet impact dynamics could be done using a constant value of contact resistance. However, predictions of the maximum splat diameter were sensitive to the value assumed. Therefore, accurate information regarding thermal contact resistance during the early stages of droplet impact is required to model droplet impact and solidification. An analytical model was developed to predict the maximum spread factor, based on equating droplet energy before and after impact, accounting for energy losses because of viscous dis-

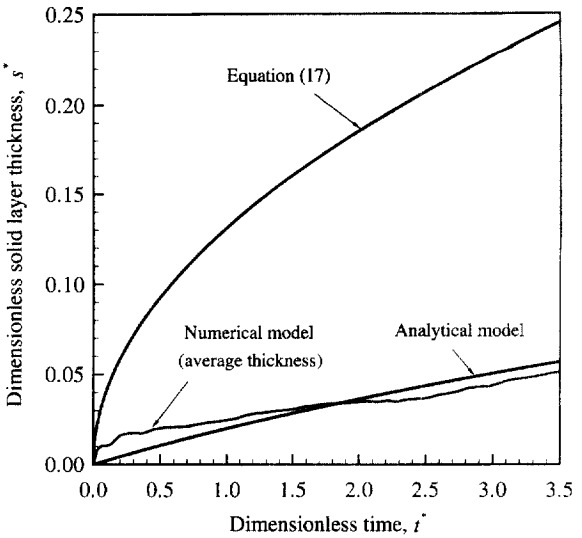

Fig. 11. Growth of the dimensionless solid layer thickness inside a tin droplet impacting a surface initially at 25 C. Predictions from the numerical model (with the thickness averaged over the droplet diameter), the analytical model of ref. [35], and from equation (17) (which neglects thermal contact resistance and assumes the surface to be isothermal) are shown.

sipation and solidification. The effect of solidification on droplet impact dynamics was found to be negligible if $\sqrt{Ste/Pr} \ll 1$.

References

[1] Vardelle M, Vardelle A, Leger AC, Fauchais P, Gobin D. Influence of particle parameters at impact on splat formation and solidification in plasma spraying process. Journal of Thermal Spraying Technology 1994;4(1):50–8.

[2] Lewis RE, Lawley A. Spray forming of metallic materials: an overview. P/M in Aerospace and Defense Technologies. Princeton: Metal Powders Industries Federation, 1991. pp. 173–84.

[3] Chen C-A, Sahu J-H, Chun J-H, Ando T. Spray forming with uniform droplets. In: Otooni MA, editor. Science and Technology Rapid Solidification and Processing. Netherlands: Kluwer Academic Publishers, 1995. pp. 123–34.

[4] Gao F, Sonin AA. Precise deposition of molten microdrops: the physics of digital microfabrication. Proceedings of the Royal Society A 1994;444:533–54.

[5] Orme M, Huang C, Courter T. Deposition strategies for control of microstructure, microporosity and surface roughness in droplet based solid freeform fabrication of structural materials. In: Matthys EF, Truckner WG, editors. Melt Spinning, Strip Casting and Slab Casting. Warrendale, PA: The Mineral, Metals and Materials Society, 1996.

[6] Schmaltz K, Amon CH. Thermal issues in microcating shape deposition manufacturing. In: Matthys EF, Truckner WG, editors. Melt Spinning, Strip Casting and Slab Casting. Warrendale, PA: The Mineral, Metals and Materials Society, 1996.

[7] Guteirrez-Miravete E. Mathematical modeling of rapid solidification. Rapid Solidification Technology, Lancaster, PA: Technomic Publishing Co. 1993. pp. 3–70.

[8] Bennet T, Poulikakos D. Heat transfer aspects of splat–quench solidification: modelling and experiment. Journal of Material Science 1994;29:2025–39.

[9] Kang B, Zhao Z, Poulikakos D. Solidification of liquid metal droplets impacting sequentially on a solid surface. ASME Journal of Heat Transfer 1994;116:436–45.

[10] Zhao Z, Poulikakos D, Fukai J. Heat transfer and fluid dynamics during the collision of a liquid droplet on a substrate—I. Modeling. International Journal of Heat and Mass Transfer 1996;39:2771–89.

[11] Zhao Z, Poulikakos D, Fukai J. Heat transfer and fluid dynamics during the collision of a liquid droplet on a substrate—II. Experiments. International Journal of Heat and Mass Transfer 1996;39:2791–802.

[12] Liu H, Lavernia EJ, Rangel R. Numerical simulation of substrate impact and freezing of droplets in plasma spray processes. Journal of Physics D: Applied Physics 1993;26:1900–8.

[13] Trapaga G, Matthys EF, Valencia JJ, Szekely J. Fluid flow, heat transfer, and solidification of molten metal droplets impinging on substrates: comparison of numerical and experimental results. Metallurgical Transactions B 1992;23B:701–918.

[14] Bertagnolli M, Marchese M, Jacucci G. Modeling of particles impacting on a rigid substrate under plasma spraying conditions. Journal of Thermal Spray Technology 1995;4:41–9.

[15] Pasandideh-Fard M, Qiao YM, Chandra S, Mostaghimi J. Capillary effects during droplet impact on a solid surface. Physics of Fluids 1996;8:650–9.

[16] Pasandideh-Fard M, Mostaghimi J. On the spreading and solidification of molten particles in a plasma spray process: effect of thermal contact resistance. Plasma Chemistry and Plasma Processing 1996;16(Supplement):83S-97S.

[17] Waldvogel JM, Poulikakos D. Solidification phenomena in picoliter size solder droplet deposition on a composite substrate. International Journal of Heat and Mass Transfer 1997;40:295–309.

[18] Madejski J. Solidification of droplets on a cold surface. International Journal of Heat and Mass Transfer 1976;19:1009–13.

[19] Madejski J. Droplets on impact with a solid surface. International Journal of Heat and Mass Transfer 1983;26:1095–8.

[20] Inada S. Transient heat transfer from a free-falling molten drop of lead to a cold plate. Journal of Chemical Engineering of Japan 1988;21:582–8.

[21] Watanabe T, Kuribayashi I, Honda T, Kanzawa A. Deformation and solidification of a droplet on a cold substrate. Chemical Engineering Science 1992;47:3059–65.

[22] Fukanuma H, Ohmori A. Behavior of molten droplets impinging on flat surfaces. Proceedings of the 7th National Thermal Spray Conference 1994. pp. 563–8.

[23] Inada S, Yang WJ. Solidification of molten metal droplets impinging on a cold surface. Experimental Heat Transfer 1994;7:93–100.

[24] Liu W, Wang GX, Matthys EF. Thermal analysis and measurements for a molten metal drop impacting on a substrate: cooling, solidification and heat transfer coefficients. International Journal of Heat and Mass Transfer 1995;38:1387–95.

[25] Nichols BD, Hirt CW, Hotchkiss RS. SOLA-VOF: a solution algorithm for transient fluid flow with multiple free boundaries Los Alamos Scientific Laboratory, LA-8355, UC-32 and UC-34, 1980.

[26] Boyer HE, Gall TL, editors, Metal Handbook. Ohio: ASM International, Materials Park, 1995.

[27] Yiding C, Faghri A, Chang WS. A numerical analysis of Stefan problems for generalized multi-dimensional phase-change structures using the enthalpy transforming model. International Journal of Heat and Mass Transfer, 1989;32:1289–98.

[28] Chabchoub F, Argyropoulos A, Mostaghimi J. Mathematical modeling and experimental measurements on the horizontal Ohno continuous casting process for pure tin. Canadian Metallurgical Quarterly 1994;33:73–88.

[29] Salcudean M, Abdullah Z. On the numerical modeling of heat transfer during solidification processes. International Journal for Numerical Methods in Engineering 1988;25:445–73.

[30] Kothe DB, Mjolsness RC, Torrey, MD. RIPPLE: a computer program for incompressible flows with free surfaces. Los Alamos National Laboratory, LA-12007-MS, 1994.

[31] Voller V, Cross M. An explicit numerical method to track a moving phase change front. International Journal of Heat Mass Transfer 1983;26:147–50.

[32] Chandra S, Avedisian CT. On the collision of a droplet with a solid surface. Proceedings of the Royal Society A 1991;432:13–41.

[33] Mills AF. Heat Transfer. Boston MA: Irwin. 1992. pp. 183–6.

[34] Ruhl RC. Cooling rates in splat cooling. Materials Science and Engineering, 1967;1:313–20.

[35] Garcia A, Clyne TW, Prates M. Mathematical model for unidirectional solidification of metals: II massive moulds. Metallurgical Transactions B 1979;10B:85–92.